Compact High-Gain Si-Imprinted THz Antenna for Ultrahigh Speed Wireless Communications

Shu-Yan Zhu, Yuan-Long Li, *Student Member, IEEE*, Kwai-Man Luk, *Fellow, IEEE,* and Stella W. Pang, *Fellow, IEEE*

***Abstract*— A low-profile and high-gain Gaussian beam antenna (GBA) operating at 1 THz is demonstrated for the first time. Imprint and dry etching technologies in silicon are employed. A complementary antenna feed based on the magnetoelectric dipole is proposed for enhancing the radiation characteristics of the antenna. The microfabrication technologies are compatible with the Si-based integrated circuit manufacturing process. The terahertz (THz) antenna is realized with over 20 dBi in antenna gain. With high-precision fabrication technologies, a highly efficient THz GBA with smooth morphology and much lower profile than conventional horn and lens antennas is developed. Moreover, the antenna has the characteristic of low sidelobe levels which is advantageous in many wireless applications.**

***Index Terms*— Gaussian beam antenna (GBA), high gain, imprint technology, low profile, Si-based microfabrication, terahertz radiation.**

I. Introduction

THE terahertz (THz) technology has attracted great interest due to its unique advantages [1]–[3] and great potential in many applications such as security inspection, medical imaging, and mobile communications. Driven by the demands of the faster data rate toward terabit-per-second (Tb/s) for future 6G networks, communications systems working at the THz band are highly desirable [4]. Antenna is one of the most important components in a wireless communication system to transmit and receive signals. Conventional THz sources have low output power, and THz waves have high propagating loss in air. Therefore, high-gain antennas are necessary for THz systems; otherwise, the distance of communications will be very limited [5], [6].

Manuscript received December 19, 2019; revised April 1, 2020; accepted April 3, 2020. Date of publication May 21, 2020; date of current version August 4, 2020. This work was supported in part by the Center for Biosystems, Neuroscience, and Nanotechnology (CBNN), City University of Hong Kong under Grant 9360148 and Grant 9380062, in part by the City University of Hong Kong Strategic Research Grant under Grant 11214517, and in part by the University Grants Council of Hong Kong GRF Projects under Grant 11247716, Grant 11218017, Grant 11213018, Grant 11212519, Grant 11219619, and CRF Project: under Grant C1013-15G. *(Corresponding author: Stella W. Pang.)*

Shu-Yan Zhu and Stella W. Pang are with the Electrical Engineering Department, City University of Hong Kong, Hong Kong, and also with the Centre for Biosystems, Neuroscience, and Nanotechnology, City University of Hong Kong, Hong Kong (e-mail: pang@cityu.edu.hk).

Yuan-Long Li and Kwai-Man Luk are with the State Key Laboratory of Terahertz and Millimeter Waves, City University of Hong Kong, Hong Kong, and also with the Electrical Engineering Department, City University of Hong Kong, Hong Kong (e-mail: eekmluk@cityu.edu.hk).

Color versions of one or more of the figures in this article are available online at http://ieeexplore.ieee.org.

Digital Object Identifier 10.1109/TAP.2020.2986863

The physical size of an antenna decreases with increasing operating frequency. Conventional manufacturing technologies for most microwave and millimeter (mm)-wave antennas will not be applicable at THz frequencies. The common horn and lens high-gain antenna operating at or above 1 THz is produced by metal milling or silicon (Si) etching technologies [7]–[10]. However, these antennas are bulky in size, with a thickness over 6 mm, and they cannot be easily integrated with planar circuits for realizing compact transceiver systems. Three-dimensional (3-D) printing technology has emerged as a promising candidate for fabricating reflectarray antennas operating between 100 and 400 GHz [11], [12]. However, the resolution of 3-D printing technology can only go down to tens of micrometers. Therefore, it is intractable to fabricate a 1 THz antenna with acceptable surface roughness using 3-D printing technologies.

Recently, microfabrication technologies were used to construct a low-profile wideband 2 × 2 magnetoelectric (ME) dipole antenna arrays operating at 1 THz by stacking multiple layers of SU-8 polymer together, each with thickness over hundreds of micrometers [13]. It is a great challenge to combine and align multiple SU-8 layers as breakage and deformation often occur during the process. The gain of the THz antenna array is 14 dBi, which indicates its high radiation efficiency. In this article, Si microfabrication technologies including deep reactive ion etching (DRIE) and imprinting were employed instead, which can provide precise dimensional control and smooth surface morphology. These technologies are compatible with Si-based integrated circuits (ICs) manufacturing technology, and the high-performance THz antenna can be integrated on the same chip with other components to form a THz device or system. In addition, applying the microfabrication technology in Si gives the advantage of providing more mechanically stable structures in Si due to its higher Young's modulus compared with SU-8 for avoiding structural deformation [14], [15].

In comparison with horn antennas, lens antennas, reflectarrays, and cavity-backed antennas, the Gaussian beam antenna (GBA) is a promising candidate to achieve both medium/high-gain performance and a low-profile structure. GBAs with a spherical concave cavity and a partially reflective surface (PRS) have been realized at microwave or mm-wave by traditional manufacturing technologies such as metal milling, electroplating, or stacked printed circuit boards (PCBs) [16], [18]. However, these technologies cannot be

applied to build 3-D spherical concave cavity structures with micrometer size. The conventional photolithography for IC fabrication cannot also be used to generate a nonplanar 3-D curved structure. Stacking multiple ring layers with different diameters together could realize a spherical concave cavity structure, but many processing steps and high precision alignments are required, as well as having the problem of forming air gaps between different layers which could reduce the radiation efficiency.

Focus ion beam (FIB), electron beam lithography (EBL), thermal scanning probe lithography (t-SPL), and imprint lithography can all be applied to fabricate 3-D micro and nanostructures [19]–[23]. Among these techniques, imprint lithography is more suitable for producing 3-D spherical concave cavity structures over a large area with fast speed, accurate dimensional control, high throughput, and low cost. Typically, FIB, EBL, or t-SPL take many hours to form a large area of 3-D microstructures by direct-write patterning, while they lack good control of the exact profile of the spherical concave cavity structure. In contrast, a spherical glass bead can be used as a stamp in imprint lithography to fabricate the spherical concave cavity with accurate dimensions and smooth curvature within a few minutes. Multiple 3-D curved cavities could be imprinted simultaneously with multiple glass beads as stamps. In this article, imprint technology is applied to fabricate the 3-D spherical concave cavity, which is then integrated with a Si-based antenna feed to realize the THz GBA. This THz GBA comprises a Si-based ME dipole antenna as the feed, a spherical concave cavity structure together with a PRS as an open resonator cavity, and a 3-D printed holder to support the PRS. With the innovation of employing the ME dipole, a kind of complementary antenna, as the antenna feed, the measured gain of this GBA is 20.3 dBi at 1.04 THz. To the best of our knowledge, this is the first time a GBA is successfully developed that can work around 1 THz. The antenna also has small thickness of about 2.5 wavelengths in free space, enabling its suitability for on-chip integration with other electronic components to form a wireless system or device for future 6G and beyond communications.

II. Design of High-Gain THz Gaussian Beam Antenna

Open resonator cavity is usually used as an optical interferometer. By changing one of the reflective surfaces to a PRS, the cavity can radiate electromagnetic waves through the PRS into free space. When the height of the cavity is an integral multiple of wavelength, resonance occurs and a highly directive beam of radiation is generated. In comparison with the conventional Fabry–Pérot cavity with two flat mirrors, the open resonator cavity (or called the spherical Fabry–Pérot cavity), with two spherical mirrors or with one flat and one spherical mirror, could support higher order Laguerre–Gaussian beam modes. More importantly, the impedance bandwidth and the 3 dB gain bandwidth of the GBA can be efficiently enhanced by exciting the hybrid fundamental mode HE_{11} with two higher order modes. This operating principle was confirmed with a practical antenna design [16], [17].

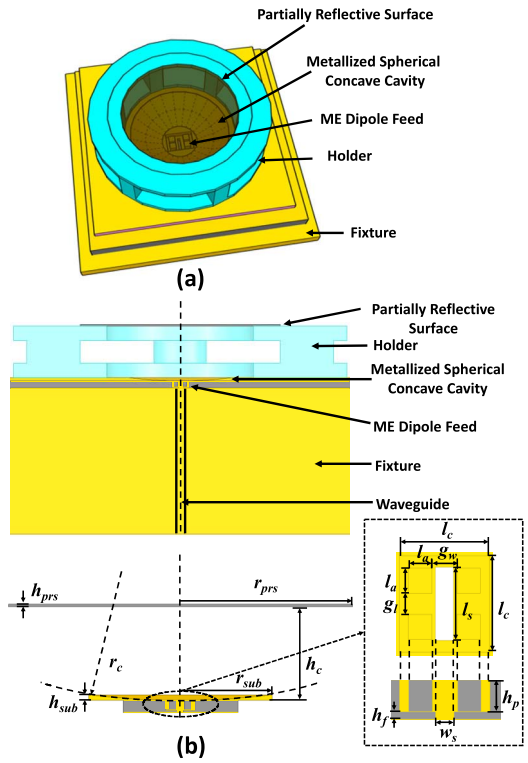

Fig. 1. (a) Schematic of THz GBA. (b) Side view of GBA and top view and side view of ME dipole feed.

TABLE I
Dimensions of THz GBA With Spherical Fabry–Pérot Cavity

Parameter	Value (μm)
h_c	750
h_{sub}	45
h_{prs}	20
r_c	7000
r_{sub}	800
r_{prs}	1500
l_c	250
l_a	65
l_s	190
w_s	50
g_l	55
g_w	70
h_f	20
h_p	80

As shown in Fig. 1(a), the proposed THz GBA consists of a metallized Si-etched ME dipole as the feed, a metallized spherical concave cavity as the reflective mirror, a 3-D printed holder, and a 20 μm-thick Si membrane as the PRS. The antenna is mounted above a metallic fixture with a WR-1.0 waveguide section at the center for convenience of measurement. Fig. 1(b) shows the side view of THz GBA as well as the top and side view of the ME dipole feed. Detailed parameters of the THz GBA are shown in Table I. According to the theory of open resonator with two spherical mirrors or one spherical mirror and one plane mirror, the resonant frequencies

of different higher order modes can be approximated by [24]

$$f_{HE} = \frac{c}{2h_c}\left[q + 1 + \frac{2p + l + 1}{\pi} \times cos^{-1}\sqrt{\left(1 - \frac{h_c}{r_c}\right)}\right] \quad (1)$$

where p, l, and q are the radial, azimuthal, and axial mode numbers, respectively; c is the speed of light; h_c is the cavity height; and r_c is the radius of curvature of the reflective mirror. As a brief review, the higher order modes can be separated into two series where the series A and series B TEM_{pl} modes of the same order have the same resonant frequency so they can be combined to synthesize the linearly polarized TEM_{pl} modes. However, in the improved open resonator theory by Luk and Yu [25], when $l > 0$, it was discovered that there is a frequency difference between the series A and series B TEM_{pl} modes of the same order and, hence, they cannot be superimposed together and there is no linearly polarized TEM_{pl} modes. A new mode designation for the open resonator was proposed with the HE_{11} mode designated as the fundamental Laguerre–Gaussian beam mode instead of TEM_{00} mode [26].

In this article, it is found that both the fundamental HE_{11} mode and the HE_{12} higher order mode can be excited in the THz GBA when the conducting plane mirror is replaced by a PRS. This is attributed to the reduction in Q-factors of the two neighboring modes. The cross-sectional magnitude and phase distributions at different axial positions are shown in Fig. 2. It can be observed that the magnitude distribution slightly below the PRS changes from a Gaussian distribution with one peak to a distribution with two symmetrical peaks around the center frequency, which confirms the excitation of both HE_{11} and HE_{12} modes. The magnitude and phase distributions at the location slightly above the PRS are relatively uniform and stable over the operating frequencies, which indicates that the mixed HE_{11} and HE_{12} modes could also generate a high-gain beam with low sidelobe level (SLL). In our design, the fifth-order cavity was chosen, which means that the height of the cavity is set to be five halves of a free-space wavelength, and the resonant frequencies of the HE_{11}, HE_{12}, and HE_{13}modes are 1.02, 1.06, and 1.1 THz, respectively. The calculated frequencies of different modes also correspond to the minimum points of S_{11} with some tolerable frequency deviation caused by cavity perturbation. The electric field (E-field) distributions of different $HE_{1,p+1}$ modes are shown in Fig. 3. Although the higher order mode could widen the bandwidth, the out-of-phase E-field across the aperture will cause gain reduction and high SLL. In this article, the HE_{11} and HE_{12} modes are excited together so a tradeoff between wide bandwidth, high gain, and low SLL can be achieved.

Conventional GBAs based on the open resonator were fed directly by an open-ended waveguide and their SLL was about -15 dB in the H-plane and -10 dB in the E-plane [16], [17]. As shown in Fig. 4(a), the radiation pattern in the E-plane is different from that in the H-plane if a WR-1.0 waveguide is used. The SLL in the E-plane of the GBA can be very high. To solve this issue, an ME dipole feed is proposed, which can reduce the difference in the E-plane and H-plane

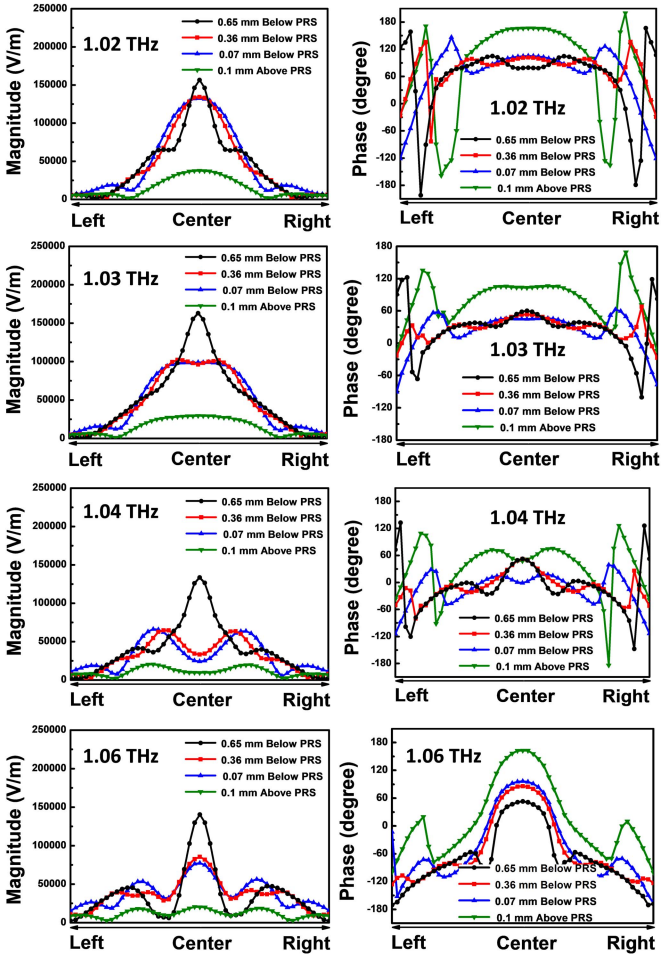

Fig. 2. Cross-sectional magnitude and phase distributions of E-field at different axial positions at 1.02, 1.03, 1.04, and 1.06 THz. The input power is 1 W.

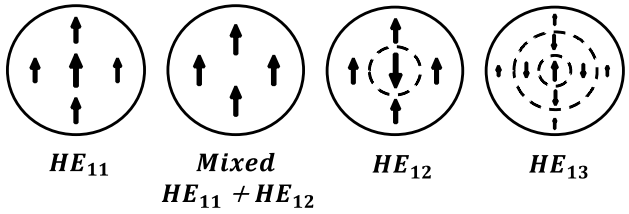

Fig. 3. Radiation patterns of $HE_{1,p+1}$ modes.

radiation patterns. As shown in Fig. 4(b), the ME dipole exhibits nearly symmetrical E-plane and H-plane radiation patterns over a wide bandwidth, which is achieved by combining an electric dipole with a magnetic dipole. The structure of this 1 THz ME dipole can be found in [13]. Besides, the ME dipole can help to reduce the SLL, improve the front-to-back ratio, and increase the gain of the THz GBA. As shown in Fig. 5, the peak SLL and the front-to-back-ratio of the GBA, fed by an ME dipole, are reduced by around 2.1 and 3.1 dB, respectively. Especially at 1.03 THz, the SLL of the radiation patterns in both E-plane and H-plane is less than -17 dB. Fig. 6(a) shows the gains versus frequency of the GBA fed by an ME dipole and an open-ended WR-1.0 waveguide. It can be seen that the gain curve of the GBA fed by an ME dipole

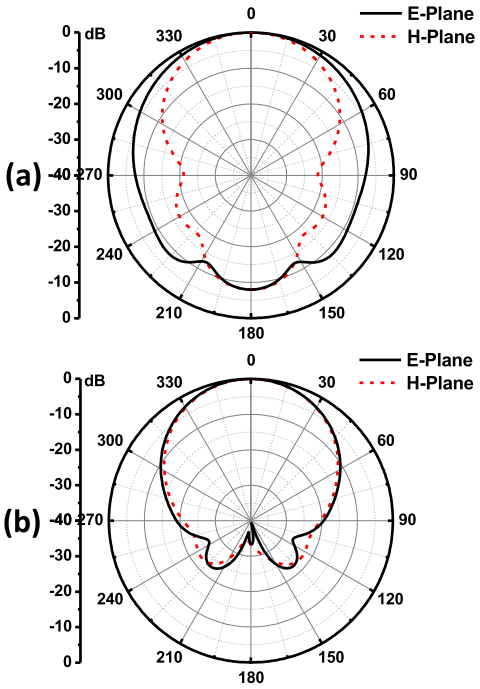

Fig. 4. Simulated radiation pattern at 1 THz for (a) waveguide WR-1.0 and (b) ME dipole.

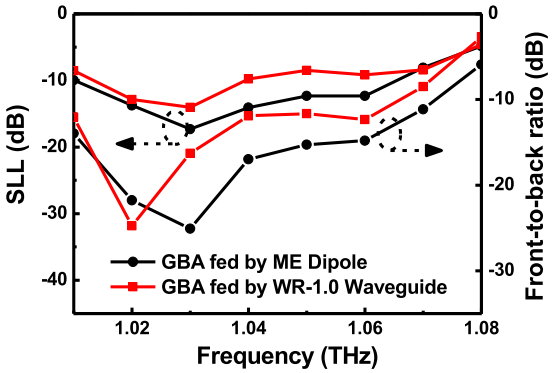

Fig. 5. SLL and front-to-back comparison between the GBA fed by waveguide and ME dipole.

within the working bandwidth from 1.02 to 1.07 THz has about 1.3 dB enhancement in average and becomes more stable over the operating frequencies. Although using the ME dipole feed does not help to improve the impedance matching or return loss of the GBA and theoretically the gain of an open resonator antenna is mainly related to the reflectivity of a PRS, the gain is also affected by the feed as the field distribution inside the cavity can be modified. As shown in Fig. 6(b), the gain of the ME dipole was about 2 dB higher than that of a WR-1.0 waveguide, which can help to reduce the spurious radiation from the open cavity and effectively increase the gain of the GBA. The maximum gain of the GBA fed by an ME dipole increased to 21.3 dB at 1.03 THz theoretically.

In addition to supporting more higher order modes, the spherical concave mirror could also help to correct the phase of the E-field across the aperture and improve the directivity. Fig. 7(a) and (b) shows the comparison of the simulated E-field magnitude distribution of the GBA with spherical and flat reflective surfaces. As shown in Fig. 7(a), the edge

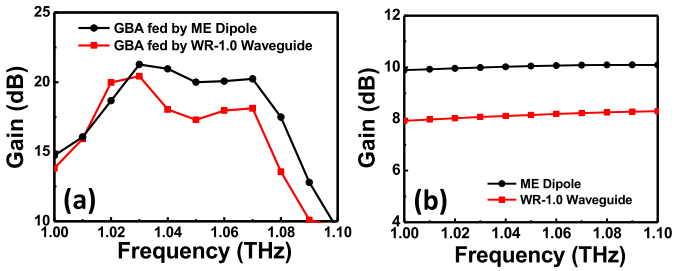

Fig. 6. (a) Simulated gain between the GBA fed by waveguide and ME dipole. (b) Simulated gain of ME dipole and WR-1.0 waveguide.

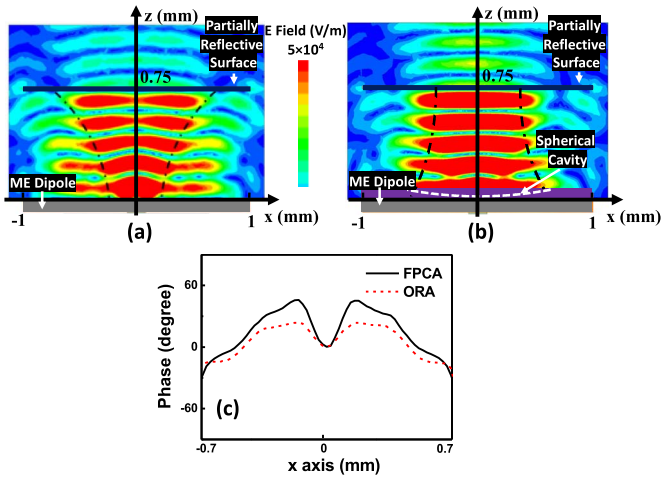

Fig. 7. E-field magnitude distribution in (a) cavity with flat reflective surface and (b) cavity with curved reflective surface. (c) E-field phase distribution along aperture diameter.

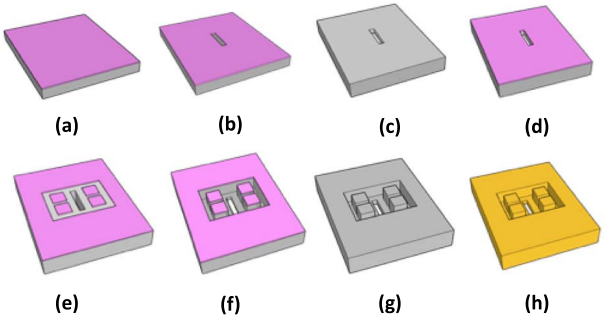

Fig. 8. Fabrication technology for Si THz antenna feed. (a) Coat resist on Si. (b) Pattern slot on Si. (c) Etch Si slot. (d) Coat resist on Si slot. (e) Pattern 4 pillars. (f) Etch 4 pillars on Si slot. (g) Remove resist. (h) Cover with Ti/Cu/Au.

radiation in the GBA with flat surface is more noticeable. In comparison, the energy can be confined more in the spherical concave cavity of the GBA. The phase distribution of the E-field along the diameter of the aperture is shown in Fig. 7(c). The phase distribution of the GBA with a spherical concave cavity is more uniform due to less edge leakage and the radiating wave is more like a plane wave, resulting in higher directivity of the antenna than the GBA with flat reflective surface.

III. Development of Imprint Technology in Si for THz Gaussian Beam Antenna

As shown in Fig. 8, the THz antenna feed was fabricated using optical lithography and Si dry etching technology.

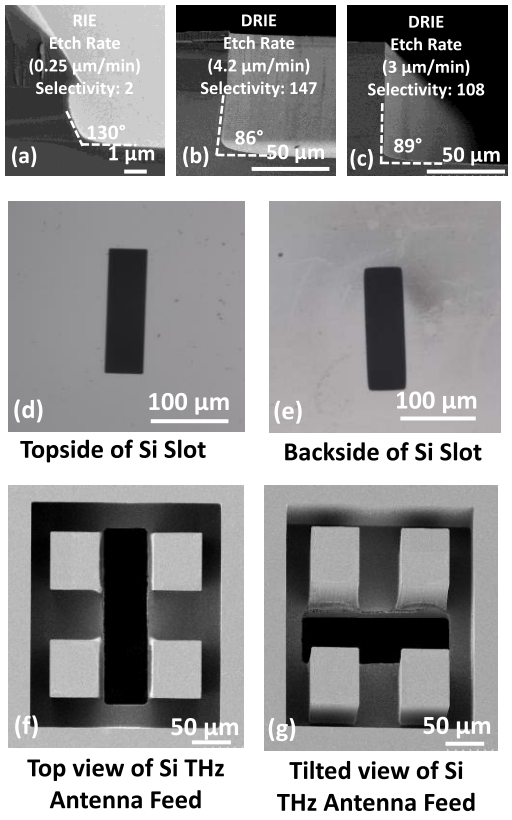

Fig. 9. (a)–(c) Profiles of Si etched under different conditions. (d) Topside and (e) backside of Si slot. (f) Top view and (g) tilted view of Si THz antenna feed.

Double side polished Si wafer with a 100 μm thickness was used as the substrate. The slot pattern with a 50 μm width and a 190 μm length was patterned by optical lithography and then used as an etch mask to etch through 100 μm-thick Si wafer using a Bosch DRIE process. This dry etching technology allowed thick layer of Si to be etched with vertical profile to achieve high aspect ratio microstructures. Subsequently, four pillar-shaped photoresist squares with a 60 μm length were aligned and patterned next to the Si slot by a high-performance mask aligner (Karl Suss MJB4; Garching, Germany). The photoresist was used as an etch mask to etch 80 μm-thick Si square pillars using the DRIE process. After removing the photoresist, 10/500/20 nm-thick titanium (Ti)/copper (Cu)/gold (Au) films were deposited on the top surface and sidewalls of the Si structure conformally by sputter deposition to metalize the Si THz antenna feed. Ti film was used as an adhesion layer and Au film was coated on the top to prevent Cu oxidation.

Fig. 9(a)–(c) shows the profiles of Si etched under different conditions. Reactive ion etching (RIE) is the most commonly used dry etching process, but the etch rate and selectivity of Si etching by RIE could be as low as 0.25 μm/min and 2, respectively. This makes it difficult to use RIE to etch Si structures with a large depth such as more than 100 μm. Besides, the photoresist is also etched and changed to tapered profile by RIE due to the low selectivity between photoresist and Si.

Instead, DRIE technology has the advantages of providing fast etch rate and high selectivity in Si patterning. The DRIE Bosch process is based on cycling between deposition and etching steps to etch Si with fast rate without undercutting while protecting the photoresist etch mask. As shown in Fig. 9(b), the Si etch rate and selectivity were improved to 4.2 μm/min and 147, respectively, by the DRIE Bosch process by switching between a passivation cycle of 85 sccm C_4F_8, 600 W coil power, and 20 mtorr for 7 s and an etch cycle of 130 sccm SF_6, 600 W coil power, 20 W platen power, and 40 mtorr for 14 s. The etch profile of the Si structures has a slope of 86°. To further improve the profile of Si structure by minimizing undercut, the etch condition was adjusted to have a passivation cycle of 85 sccm C_4F_8, 600 W coil power, and 16 mtorr for 5 s and an etch cycle of 120/13 sccm SF_6/O_2, 600 W coil power, 14 W platen power, and 30 mtorr for 8 s. The etch rate and selectivity were decreased to 3 μm/min and 108, respectively, but the etch profile became more vertical at 89°, which is suitable for the high-performance Si THz antenna feed with thickness over one hundreds of micrometers.

Fig. 9(d) and (e) shows the front and back sides of the Si slot, respectively. The measured Si slot had a 50 μm width, a 190 μm length, and a 100 μm thickness. As the slot was etched through vertically, the size of the front and back sides was the same. Top and tilted views of the Si THz antenna feed coated with 10/500/20 nm Ti/Cu/Au films are shown in Fig. 9(f) and (g). Due to the well-controlled etch profile and smooth etch condition, the etched surface of the Si THz antenna was smooth with high dimensional accuracy. No deformation was observed for the Si THz antenna since Si has a high Young's modulus. The surface smoothness of the antenna is important to ensure high efficiency. Antennas in SU-8 polymer and Si before and after metallization were evaluated for their surface morphology using an atomic force microscope (AFM). As shown in Fig. 10, before metal deposition, the surface roughness of Si was found to be 0.29 nm, lower than 0.35 nm shown in the SU-8 polymer. After the THz antennas were metalized with Ti/Cu/Au films, the surface roughness of the metal surface increased to 1.20 and 1.94 nm on Si and SU-8, respectively. Microfabricated THz antennas had much smoother surface morphology, in the order of 1–2 nm, compared with antennas made by 3-D printing or metal milling, which typically have surface roughness in the order of 0.38 μm. The smooth surface formed in the THz antennas substantially improves their performance in the THz range with low loss and high efficiency.

An important element for THz GBA is the formation of 3-D spherical concave cavity structure with height variation up to 100 μm. Conventional IC manufacturing processes are designed for planar devices and often limit to height of just a few micrometers. Although stacking multiple ring structures could result in a curved cavity, it requires very precise alignment and the curvature is formed by multiple steps instead of having a smooth spherical surface. To fabricate a smooth spherical concave cavity with high accuracy, imprint technology with glass bead was used [27]–[29]. As shown in Fig. 11, a glass bead was used as a stamp to imprint photoresist on glass. The imprint process was carried out at 95 °C and 5 bar for 10 min, and 395 nm ultraviolet (UV) exposure for 2 min [30]. After demolding the glass

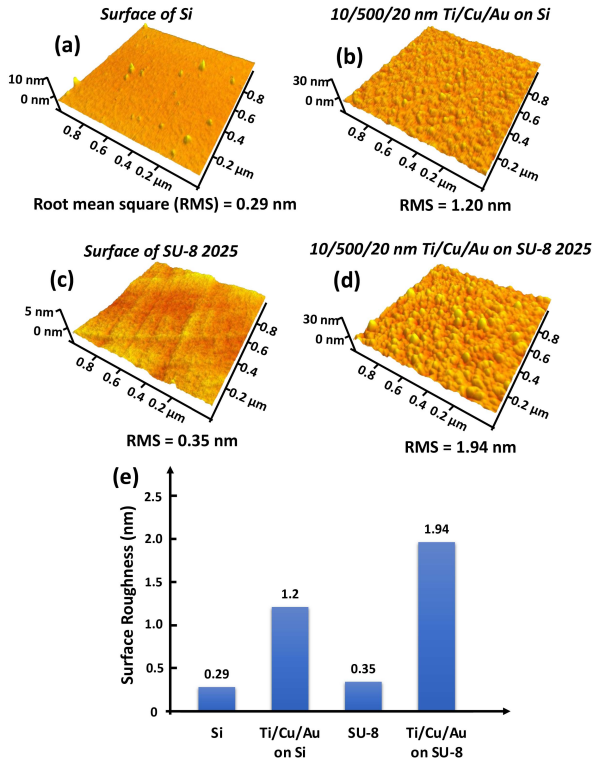

Fig. 10. Atomic force micrographs of (a) Si, (b) Ti/Cu/Au on Si, (c) SU-8, and (d) Ti/Cu/Au on SU-8 surfaces. (e) Comparison of surface roughness for Si and SU-8 before and after Ti/Cu/Au deposition.

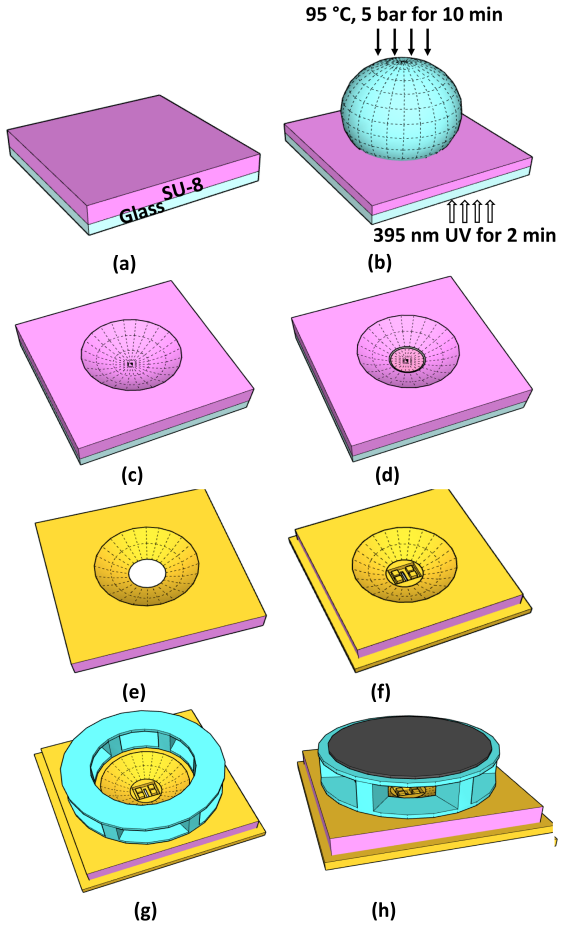

Fig. 11. Fabrication technology for THz antenna with spherical Fabry–Pérot cavity. (a) Coat SU-8 on glass. (b) Imprint SiO_2 bead on SU-8. (c) Remove SiO_2 bead. (d) Drill hole in center by laser cutting. (e) Coat Ti/Cu/Au and peel off. (f) Stack curved structure on top of antenna feed. (g) Put holder above curved structure. (h) Place 20 μm thick, 3 mm diameter Si membrane above holder.

bead at 20 °C, a spherical concave cavity was generated in the SU-8 over the glass substrate. A femtosecond laser system was used to drill a 450 μm diameter circle at the central of the spherical concave cavity. Subsequently, 10/500/20 nm-thick Ti/Cu/Au films were deposited on the spherical concave cavity by sputter-deposition. The metalized cavity was then peeled off from the glass substrate and adhered on top of the Si THz antenna feed. The alignment between the curved cavity and the Si antenna feed was done under a long working distance microscope. A polymer holder with a 2 mm inner diameter and a 4 mm outer diameter was fabricated by 3-D printing, and it was placed on top of the metallized cavity. A 1-inch diameter undoped ultrathin Si membrane (Virginia Semiconductor Inc., Fredericksburg, VA, USA) with a 20 μm thickness was cut to a 3 mm diameter by a femtosecond laser with 850 μW power. The 3 mm diameter Si membrane was then placed on top of the polymer holder under the long working distance microscope. The three-layer unit with an SU-8 curved cavity, a polymer holder, and a 3 mm diameter Si membrane was fixed together using a thin layer of SU-8 polymer at 80 °C for 1 min and then cross-linked by UV exposure at 20 °C for 1 min. Fig. 12(a) shows the formation of a spherical concave cavity by imprinting a glass bead with a 14 mm diameter into a layer of polymer. After the imprint, the resulting spherical cavity would have a diameter of 1584 μm and a depth of 45 μm, which met the GBA design requirements. Fig. 12(b) shows the micrographs of spherical concave cavities with different dimensions after imprinting. As shown in Fig. 12(b1)–(b3), polydimethylsiloxane (PDMS) polymer with an initial thickness of 31 μm on glass resulted in a PDMS spherical concave cavity with 2530 μm in diameter and 118 μm in depth. During the imprint process, the PDMS polymer flowed and accumulated around the edges of the glass bead and hardened by annealing at 110 °C for 10 min. When the initial thickness of PDMS polymer was reduced to 16 μm, the diameter and depth of the PDMS cavity was reduced to 2020 and 73 μm, respectively. However, these dimensions were different from the desired spherical concave cavity structure and further decrease of PDMS thickness caused difficulty in peeling off the PDMS polymer from the glass as well as structural deformation.

In comparison, the SU-8 polymer with the same initial thickness resulted in a spherical concave cavity with smaller diameter and lower depth due to its higher viscosity (5485 centipoises for SU-8 2025 versus 3500 centipoises for PDMS mixed at 10:1 curing ratio). Besides, SU-8 is a more rigid polymer with Young's modulus that is 2.6×10^4 times higher than PDMS, which prevents deformation of the microstructure or wrinkle formation during the peel off process. As shown in Fig. 12(b4)–(b6), the SU-8 2025 with an initial thickness of 16.5 μm generated a curved cavity with 1580 μm in diameter and 44 μm in depth, which satisfied the dimensions required for the THz GBA. Fig. 13 shows

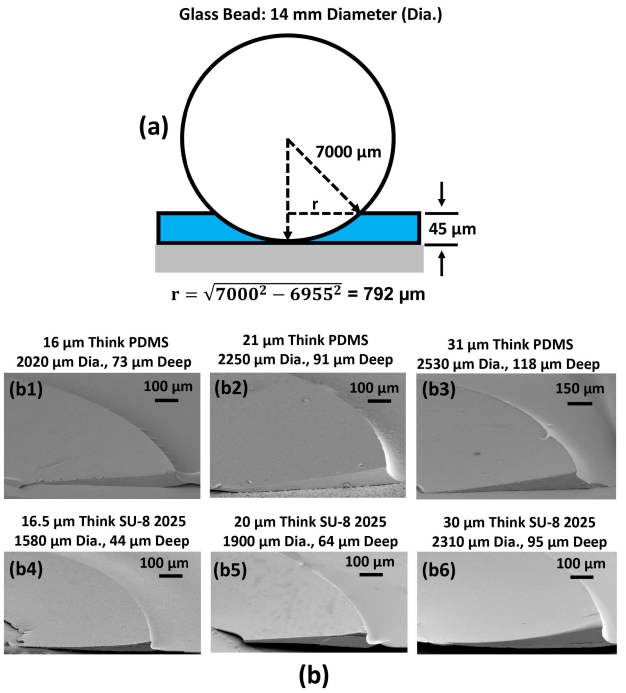

Fig. 12. (a) Formation of spherical concave cavity by imprinting glass bead with a 14 mm diameter into polymer. (b) Micrographs of curved cavities with different dimensions due to various initial PDMS and SU-8 thicknesses.

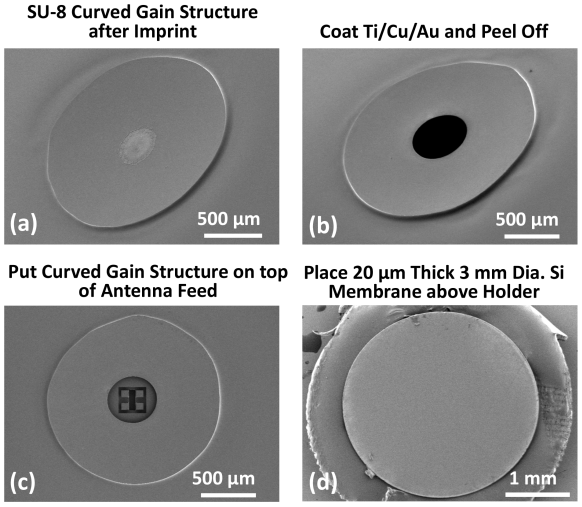

Fig. 13. Micrographs of (a) curved cavity structure after imprint, (b) curved cavity with hole in center and coated with Ti/Cu/Au, (c) curved cavity structure stacked on top of antenna feed, and (d) top view of THz resonator antenna with a 20 μm thick and 3 mm diameter Si membrane above holder.

the micrographs of the THz GBA during different stages of fabrication. In Fig. 13(a), the 3-D curved cavity with the desired dimensions was formed after imprinting using the glass bead. After coating with Ti/Cu/Au, the 3-D curved cavity with a hole in center is shown in Fig. 13(b). Fig. 13(c) shows the curved cavity stacked on top of the Si antenna feed. The entire THz GBA was completed by placing a 20 μm thick, 3 mm diameter Si membrane above holder as part of the spherical concave cavity, as shown in Fig. 13(d).

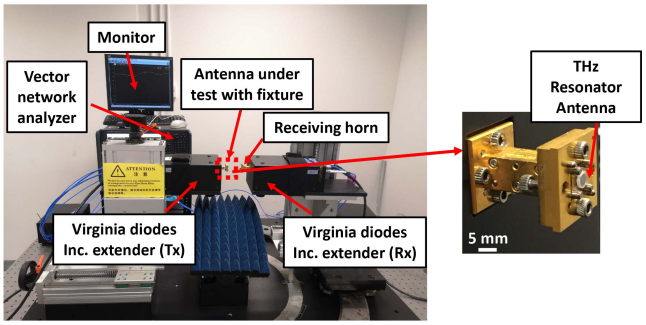

Fig. 14. THz antenna measurement system.

IV. Performance of Terahertz High-Gain Gaussian Beam Antenna

Fig. 14 shows the antenna measurement setup. A THz in-house far-field measurement system was used to measure the scattering (S) parameters. The system consists of a vector network analyzer (VNA, Agilent N8245A), a pair of Virginia Diodes Inc. (VDI) extenders, a monitor, and a manual turntable. Two VDI extenders were used as the THz sources operating from 0.75 to 1.1 THz. The fabricated THz GBA together with a supporting fixture was mounted on the WR-1.0 waveguide flange of the VDI extender (T_x). A WR-1.0 diagonal horn was connected to another VDI extender (R_x) as a receiving antenna and fixed on the manual turntable. The whole system was installed on a vibration-free platform to reduce possible errors. Before taking the measurement, the short-open-load-through calibration was performed by the VDI WR-1.0 calibration kit. Laser alignment was used to ensure that the fabricated antenna and the receiving antenna were at the same level. The metallic surfaces of the measurement system were covered with absorbers to reduce multiple reflection. The plot of the reflection coefficient as a function of frequency was directly read from the VNA. The plot of gain as a function of frequency was obtained by comparing S_{21} of the antenna under test (AUT) and a commercial THz horn with 22 dBi gain, estimated by the manufacturer. When measuring the radiation pattern, the AUT was mounted on the turntable which could be rotated horizontally around the center point, and the angular movement was limited to $\pm 60°$ with a precision of 1°. For far-field measurements, the distance between the AUT and the receiving horn was set at 80 mm, which is larger than the Fraunhofer distance of 60 mm.

Fig. 15 shows the simulated and measured reflection coefficients of the THz GBA. It can be seen that the simulated S_{11} was below -10 dB from 1.02 to 1.08 THz. The trend of the measured S_{11} matched well with the simulated results, but the measured S_{11} was much lower in value. To investigate the reasons, the effect of having an air gap between the curved SU-8 cavity and the Si antenna feed was considered. Simulations with 50/100/500 nm gap were studied and the results reveal that S_{11} of three gaps were the same as the ideal surface contact, which means air gap up to 500 nm is a tolerable variation. Another possible reason is that the metallic fixture could cause additional energy loss. To better understand

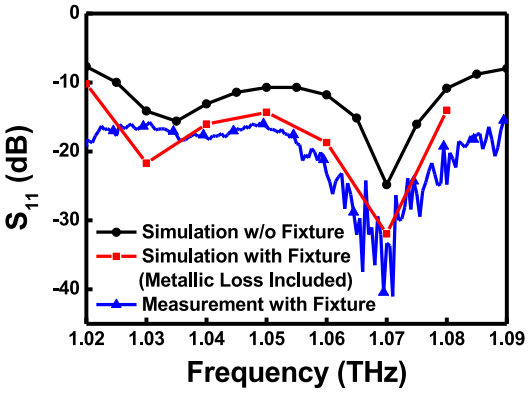

Fig. 15. Simulated and measured reflection coefficient, S_{11}, for THz resonant antenna with spherical Fabry–Pérot cavity.

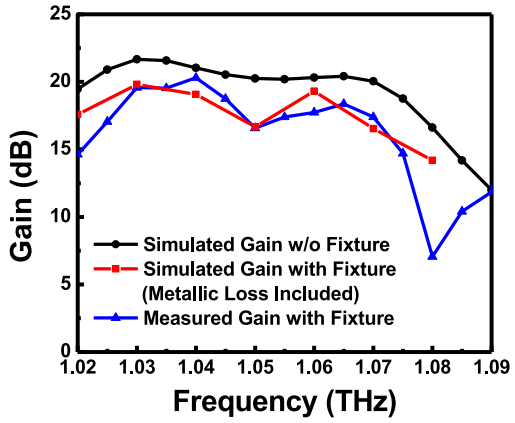

Fig. 16. Simulated and measured gain for THz resonant antenna with spherical Fabry–Pérot cavity.

its influence on the antenna performance, the loss due to the metallic fixture was considered and added in the simulation model. The metallic fixture consisted of four location pins around the antenna and a bulky rectangular base with a waveguide slot in the center to connect the waveguide port on the T_x and the antenna. All the conductors were assumed to have finite conductivity in the model. The surface roughness of the machined metallic fixture and the microfabricated antenna was 1.1 μm and 2.0 nm, respectively, which were measured by AFM. As shown in Fig. 15, there is an obvious downward trend of the simulated S_{11} of the antenna when the metallic loss of the fixture was included in the simulation and it shows a better agreement with the measured results. Therefore, the difference may be mainly caused by metallic loss from the sample and the metallic fixture. In particular, the metallic loss due to the waveguide section of the metallic fixture is substantial.

The simulated gain without and with the fixture, and the measured gain of the THz GBA with the fixture are shown in Fig. 16. It can be observed that the trend of the measured gain agrees well with the simulated one in the THz band. The measured peak gain of the THz GBA is 20.3 dBi at 1.04 THz, and the measured standing wave ratio (SWR) is less than 2 from 1.02 to 1.07 THz. To investigate the effects of surface variation of the spherical cavity on the performance

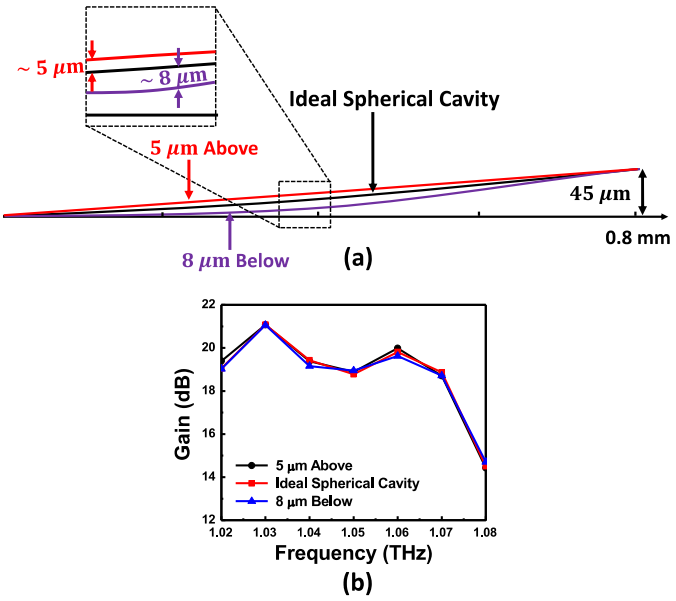

Fig. 17. (a) Schematic and (b) simulated gain of two spherical cavities with surface variation of 5 μm above and 8 μm below ideal surface.

of THz GBA, two different cavities with surface variation over 5 μm were simulated, and the result is shown in Fig. 17. Through the simulation, it is found that the performances of the antenna are not sensitive to the curvature of the cavity within a few micrometers difference, so the variation of the fabricated cavity is tolerable. This further confirms that the differences between the simulated and measured gain curves, as shown in Fig. 16, are due to the metallic loss in the mounting fixture.

The radiation pattern was measured by the antenna measurement system, as shown in Fig. 14. The measured angle was limited to $\pm 60^\circ$ due to the limitation of the system. Fig. 18(a) and (b) shows the simulated and measured radiation patterns of the GBA at 1.03 THz in the E-plane and H-plane, respectively. Without the mounting fixture, the antenna has -17.3 dB SLL in the E-plane and -18.8 dB SLL in the H-plane by simulation. With the fixture, there is a little deterioration in SLL but still lower than -16 dB in all planes, again by simulation. The measured main beams in the E-plane and H-plane have a good agreement with the simulated results with and without fixtures, indicating that the THz GBA with a spherical curved cavity could achieve a highly directive radiation. The general trend of the measured SLL is the same as the simulated results, but the fluctuation in the curves is probably due to two main reasons. The first one is related to the power receiving by the antenna which is weak due to low source power and high propagation loss. Fig. 18 shows the normalized noise floor level (with long enough integration time) of S_{21} at 1.03 THz from the VNA measurement. As the noise floor level of the VNA was not much lower than the receiving power, the value of S_{21} could not be accurately measured. Another reason is that the coaxial cables connecting to the VDI extenders were very sensitive. When measuring the SLL, the cable could be over-stretched, and the accuracy was affected. The measured 3 dB beamwidths in the H-plane

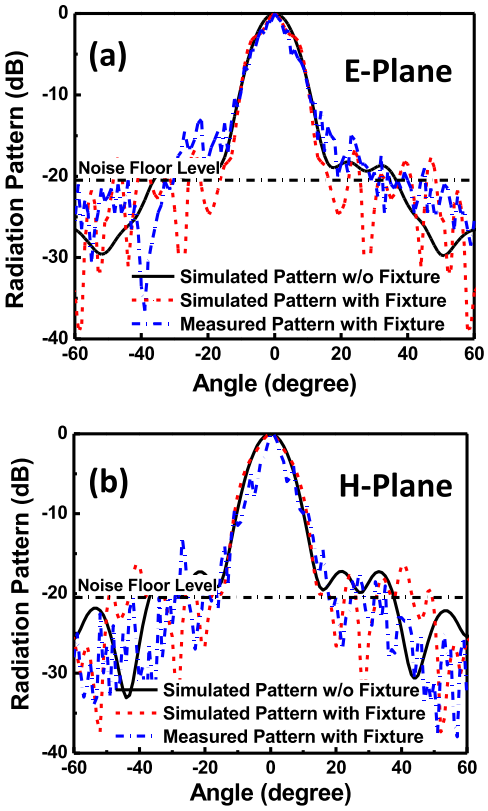

Fig. 18. Simulated and measured radiation patterns in (a) E-plane and (b) H-plane for THz GBA with spherical Fabry–Pérot cavity.

and E-plane were about 12° at 1.04 THz, agreeing well with the simulated results. Therefore, the simulated directivity could be used to estimate the radiation efficiency. Using the ratio between gain and directivity, the radiation efficiency at 1.04 THz is about 73%.

V. Conclusion

A high-gain and low-profile THz GBA has been realized by the imprint and dry etching technologies in Si. An ME dipole was proposed as the antenna feed which was etched by the DRIE process that can provide high aspect ratio microstructures in Si with smooth morphology. Imprint technology was developed to fabricate the 3-D curved cavity structure in PDMS and SU-8 2025 polymers. It demonstrates that SU-8 2025 with an initial thickness of 16.5 μm can produce a spherical curved cavity with a very smooth surface and the required dimensions of 1580 μm in diameter and 44 μm in depth. The spherical curved cavity and the PRS are separated by a 3-D printed holder to form the THz antenna. The measured peak gain of the THz antenna is 20.3 dBi at 1.04 THz, and the measured 3 dB bandwidth was 50 GHz, with SWR less than 2 from 1.02 to 1.07 THz. The measured main beam in the E-plane and H-plane matched well with the simulated results, confirming that low SLL and high gain can be achieved by this low-profile THz GBA.

Acknowledgment

The authors would like to thank Dr. Kam-Man Shum, Dr. Ka-Fai Chan, and Chun-Ka Lau for their help to set up the terahertz (THz) measurement system, 3-D printed the polymer holder, and fabricated the fixture, respectively. They would also like thank the Technical Staff at the CBNN, State Key Laboratory of Terahertz and Millimeter Waves, and Optoelectronics Laboratory, City University of Hong Kong, Hong Kong, for their technical support.

References

[1] K. Wu, Y. J. Cheng, T. Djerafi, and W. Hong, "Substrate-integrated millimeter-wave and terahertz antenna technology," *Proc. IEEE*, vol. 100, no. 7, pp. 2219–2232, Jul. 2012.

[2] K. Sengupta, T. Nagatsuma, and D. M. Mittleman, "Terahertz integrated electronic and hybrid electronic–photonic systems," *Nature Electron.*, vol. 1, no. 12, pp. 622–635, Dec. 2018.

[3] P. Mukherjee and B. Gupta, "Terahertz (THz) frequency sources and antennas–A brief review," *Int. J. Infr. Millim. Waves*, vol. 29, no. 12, pp. 1091–1102, Dec. 2008.

[4] T. S. Rappaport *et al.*, "Wireless communications and applications above 100 GHz: Opportunities and challenges for 6G and beyond," *IEEE Access*, vol. 7, pp. 78729–78757, 2019.

[5] K. R. Jha and G. Singh, "Terahertz planar antennas for future wireless communication: A technical review," *Infr. Phys. Technol.*, vol. 60, pp. 71–80, Sep. 2013.

[6] T. Kleine-Ostmann and T. Nagatsuma, "A review on terahertz communications research," *J. Infr., Millim., Terahertz Waves*, vol. 32, no. 2, pp. 143–171, Feb. 2011.

[7] A. Gonzalez, K. Kaneko, T. Kojima, S. I. Asayama, and Y. Uzawa, "Terahertz corrugated horns (1.25–7 THz): Design, Gaussian modeling, and measurements," *IEEE Trans. Terahertz Sci. Technol.*, vol. 7, no. 1, pp. 1–11, 2016.

[8] M. Alonso-delPino, T. Reck, C. Jung-Kubiak, C. Lee, and G. Chattopadhyay, "Development of silicon micromachined microlens antennas at 1.9 THz," *IEEE Trans. Terahertz Sci. Technol.*, vol. 7, no. 2, pp. 191–198, Mar. 2017.

[9] N. Llombart *et al.*, "Silicon micromachined lens antenna for THz integrated heterodyne arrays," *IEEE Trans. Terahertz Sci. Technol.*, vol. 3, no. 5, pp. 515–523, Sep. 2013.

[10] H.-T. Zhu, Q. Xue, J.-N. Hui, and S. W. Pang, "A 750–1000 GHz *H*-plane dielectric horn based on silicon technology," *IEEE Trans. Antennas Propag.*, vol. 64, no. 12, pp. 5074–5083, Dec. 2016.

[11] Z.-W. Miao, Z.-C. Hao, Y. Wang, B.-B. Jin, J.-B. Wu, and W. Hong, "A 400-GHz high-gain quartz-based single layered folded reflectarray antenna for terahertz applications," *IEEE Trans. Terahertz Sci. Technol.*, vol. 9, no. 1, pp. 78–88, Jan. 2019.

[12] P. Nayeri *et al.*, "3D printed dielectric reflectarrays: Low-cost high-gain antennas at sub-millimeter waves," *IEEE Trans. Antennas Propag.*, vol. 62, no. 4, pp. 2000–2008, Apr. 2014.

[13] K. M. Luk *et al.*, "A microfabricated low-profile wideband antenna array for terahertz communications," *Sci. Rep.*, vol. 7, no. 1, p. 1268, Dec. 2017.

[14] H.-T. Zhu, Q. Xue, J.-N. Hui, and S. W. Pang, "Design, fabrication, and measurement of the low-loss SOI-based dielectric microstrip line and its components," *IEEE Trans. Terahertz Sci. Technol.*, pp. 1–10, 2016.

[15] W. Withayachumnankul, R. Yamada, M. Fujita, and T. Nagatsuma, "All-dielectric rod antenna array for terahertz communications," *APL Photon.*, vol. 3, no. 5, May 2018, Art. no. 051707.

[16] F. Wu and K. M. Luk, "Wideband high-gain open resonator antenna using a spherically modified, second-order cavity," *IEEE Trans. Antennas Propag.*, vol. 65, no. 4, pp. 2112–2116, Apr. 2017.

[17] Q.-Y. Guo and H. Wong, "Wideband and high-gain Fabry–Pérot cavity antenna with switched beams for millimeter-wave applications," *IEEE Trans. Antennas Propag.*, vol. 67, no. 7, pp. 4339–4347, Jul. 2019.

[18] Q. Chen, X. Chen, and K. Xu, "3-D printed Fabry–Pérot resonator antenna with paraboloid-shape superstrate for wide gain bandwidth," *Appl. Sci.*, vol. 7, no. 11, pp. 1134–1145, 2017.

[19] D. López-Romero, C. A. Barrios, M. Holgado, M. F. Laguna, and R. Casquel, "High aspect-ratio SU-8 resist nano-pillar lattice by e-beam direct writing and its application for liquid trapping," *Microelectron. Eng.*, vol. 87, no. 4, pp. 663–667, Apr. 2010.

[20] Y. Lisunova, M. Spieser, R. D. D. Juttin, F. Holzner, and J. Brugger, "High-aspect ratio nanopatterning via combined thermal scanning probe lithography and dry etching," *Microelectron. Eng.*, vol. 180, pp. 20–24, Aug. 2017.

[21] W. Li *et al.*, "Three-dimensional nanostructures by focused ion beam techniques: Fabrication and characterization," *J. Mater. Res.*, vol. 28, no. 22, pp. 3063–3078, Nov. 2013.
[22] S. Zhu, H. Li, M. Yang, and S. W. Pang, "Highly sensitive detection of exosomes by 3D plasmonic photonic crystal biosensor," *Nanoscale*, vol. 10, no. 42, pp. 19927–19936, 2018.
[23] S. Zhu, H. Li, M. Yang, and S. W. Pang, "Label-free detection of live cancer cells and DNA hybridization using 3D multilayered plasmonic biosensor," *Nanotechnology*, vol. 29, no. 36, pp. 365503–365516, 2018.
[24] K. M. Luk, "Generalised open resonator theory," *IEE Proc. J-Optoelectron.*, vol. 133, no. 4, pp. 293–298, Aug. 1986.
[25] K.-M. Luk and P.-K. Yu, "Complex-source-point theory of Gaussian beams resonators," *IEE Proc. J-Optoelectron.*, vol. 132, no. 2, pp. 105–113, Apr. 1985.
[26] K.-M. Luk and P.-K. Yu, "Mode designations of laser beams," *IEE Proc. J-Optoelectron.*, vol. 132, no. 3, pp. 191–194, Jun. 1985.
[27] L. R. Bao, X. Cheng, X. D. Huang, L. J. Guo, S. W. Pang, and A. F. Yee, "Nanoimprinting over topography and multilayer three-dimensional printing," *J. Vac. Sci. Technol. B, Microelectron.*, vol. 20, no. 6, pp. 2881–2886, 2002.
[28] W. Hu, B. Yang, C. Peng, and S. W. Pang, "Three-dimensional SU-8 structures by reversal UV imprint," *J. Vac. Sci. Technol. B, Microelectron. Nanometer Struct. Process., Meas., Phenomena*, vol. 24, no. 5, pp. 2225–2229, 2006.
[29] C. Peng, B. L. Cardozo, and S. W. Pang, "Three-dimensional metal patterning over nanostructures by reversal imprint," *J. Vac. Sci. Technol. B, Microelectron.*, vol. 26, no. 2, pp. 632–635 2008.
[30] S. Zhu, H. Li, M. Yang, and S. W. Pang, "High sensitivity plasmonic biosensor based on nanoimprinted quasi 3D nanosquares for cell detection," *Nanotech.*, vol. 27, no. 29, pp. 295101–295113, 2016.

Shu-Yan Zhu was born in Hubei, China, in 1988. He received the B.Eng. degree from the Department of Electronic Science and Technology, Southwest University, Chongqing, China, in 2009, the M.Phil. degree in material physics and chemistry from the Department of Electronic Science and Technology, Huazhong University of Science and Technology, Wuhan, China, in 2014, and the Ph.D. degree from the Department of Electrical Engineering, City University of Hong Kong, Hong Kong, in 2019.

He is currently a Research Fellow with the Center for Biosystems, Neuroscience, and Nanotechnology, City University of Hong Kong. His current research interests include terahertz (THz) and nanoplasmonics device, nanofabrication technology, and optofluidic lab-on-chip device.

Yuan-Long Li (Student Member, IEEE) was born in Lanzhou, China, in 1995. He received the B.Sc. (Eng.) degree in radio wave propagation and antenna from the University of Electronic Science and Technology of China, Chengdu, China, in 2014. He is currently pursuing the Ph.D. degree in electrical engineering with the City University of Hong Kong, Hong Kong.

His current research interests include open resonator antennas and terahertz antennas.

Kwai-Man Luk (Fellow, IEEE) received the B.Sc. (Eng.) and Ph.D. degrees in electrical engineering from The University of Hong Kong, Hong Kong, in 1981 and 1985, respectively.

In 1985, he joined the Department of Electronic Engineering, City University of Hong Kong, Hong Kong, as a Lecturer. Two years later, he moved to the Department of Electronic Engineering, The Chinese University of Hong Kong, Hong Kong, where he spent four years. In 1992, he returned to the City University of Hong Kong, where he served as the Head of the Department of Electronic Engineering from 2004 to 2010 and the Director of the State Key Laboratory of Millimeter Waves from 2008 to 2013, and he is currently the Chair Professor of electronic engineering. He has authored over 4 books, 11 research book chapters, over 380 journal articles, and 250 conference articles. He was awarded 10 U.S. and more than 10 PRC patents on the design of a wideband patch antenna with an L-shaped probe feed. His recent research interests include design of patch antennas, magnetoelectric dipole antennas, dense dielectric patch antennas, and open resonator antennas for various wireless applications.

Dr. Luk is a fellow of the U.K. Royal Academy of Engineering. He received the Japan Microwave Prize at the 1994 Asia–Pacific Microwave Conference held in Chiba in December 1994, the Best Paper Award at the 2008 International Symposium on Antennas and Propagation held in Taipei in October 2008, the Best Paper Award at the 2015 Asia–Pacific Conference on Antennas and Propagation held in Bali in July 2015, the very competitive 2000 Croucher Foundation Senior Research Fellow in Hong Kong, the 2011 State Technological Invention Award (2nd Honor) of China, and the 2017 IEEE APS John Kraus Antenna Award. He was conferred the 2019 Prize for Scientific and Technological Progress in the category of electronics and information technology by the Ho Leung Ho Lee Foundation. He was the Technical Program Chairperson of the 1997 Progress in Electromagnetics Research Symposium (PIERS), a General Vice Chairperson of the 1997 and 2008 Asia–Pacific Microwave Conference (APMC), a General Chairman of the 2006 IEEE Region Ten Conference (TENCON), the Technical Program Co-Chairperson of the 2008 International Symposium on Antennas and Propagation (ISAP), the General Co-Chairperson of the 2011 IEEE International Workshop on Antenna Technology (IWAT), a General Co-Chair of the 2014 IEEE International Conference on Antenna Measurements and Applications (CAMA), and a General Co-Chair of the 2015 International Conference on Infrared, Millimeter, and Terahertz Waves (IRMMW-THz 2015). He is the General Chair of the 2020 Asia–Pacific Microwave Conference to be held in Hong Kong in November 2020.

Stella W. Pang (Fellow, IEEE) received the B.Sc. degree from Brown University, Providence, RI, USA, in 1977, and the M.Sc. and Ph.D. degrees from Princeton University, Princeton, NJ, USA, in 1978 and 1981, respectively.

From 1981 to 1989, she was with the Lincoln Laboratory, Massachusetts Institute of Technology, Cambridge, MA, USA. From 1990 to 2011, she was a Professor of electrical engineering and computer science and also the Associate Dean of the Graduate Education and International Programs with the College of Engineering, University of Michigan, Ann Arbor, MI, USA, from 2002 to 2007. She is currently a Chair Professor and the Head of the Department of Electrical Engineering, City University of Hong Kong, Hong Kong, where she is also the Director of the Center for Biosystems, Neuroscience, and Nanotechnology. She has over 400 technical articles, book chapters, and invited presentations and is the editor and an author of 16 books, journals, and conference proceedings. She has nine patents granted in nanotechnology and microsystems. Her research interests include nanofabrication technology for biomedical, microelectromechanical, microelectronic, and optical devices.

Dr. Pang is a Fellow of the Electrochemical Society (ECS), the American Vacuum Society (AVS), and the Hong Kong Institution of Engineers (HKIE). She has served as a Conference Organizer for AVS, ECS, the IEEE Electronic Materials Conference, the International Symposium on Electron, Ion, and Photon Beam Technology, and Nanofabrication, the Material Research Society, and SPIE. She has taught 32 short courses on microfabrication and nanoimprint technology for microelectronic manufacturing and microelectromechanical systems.